Chemosphere 217 (2019) 780–789

Contents lists available at ScienceDirect

Chemosphere

journal homepage: www.elsevier.com/locate/chemosphere

Electrochemical oxidation of gaseous benzene on a Sb-SnO_2/foam Ti nano-coating electrode in all-solid cell

Bo Zhang [a], Min Chen [a], Changbin Zhang [a, b, *], Hong He [a, b, c]

[a] State Key Joint Laboratory of Environment Simulation and Pollution Control, Research Center for Eco-Environmental Sciences, Chinese Academy of Sciences, Beijing 100085, China
[b] University of Chinese Academy of Sciences, Beijing 100049, China
[c] Center for Excellence in Regional Atmospheric Environment, Institute of Urban Environment, Chinese Academy of Sciences, Xiamen 361021, China

HIGHLIGHTS

- Sb-SnO_2/Ti nano-coating anode was firstly applied on oxidation of gaseous aromatics.
- Benzene was oxidized to CO_2 with selectivity of 85% without any organic byproducts.
- Electrode with loading of 7.7 mg cm^{-2} and 14.0 mol% Sb shows the excellent activity.
- Continuous supplies of vapor to the reactant is important to oxidation of benzene.
- Electroactive surface and reaction rate were response for the activity of electrode.

ARTICLE INFO

Article history:
Received 26 July 2018
Received in revised form
23 October 2018
Accepted 31 October 2018
Available online 10 November 2018

Handling Editor: E. Brillas

Keywords:
Electrochemical oxidation
Indoor air pollution
Benzene
Volatile organic compounds

ABSTRACT

An all-solid cell with a solid polymer electrolyte was applied to electrochemical oxidation of low-concentration indoor gaseous aromatic pollution. Antimony-doped tin dioxide nanocoatings deposited on a titanium foam substrate (Ti/Sb-SnO_2) with different Sb/Sn ratios (4.8–14.0 mol%) and loading weight of Sb-SnO_2 (4.4–7.7 mg cm^{-2}) were used as dimensionally stable anodes. Sn and Sb were homogeneously dispersed on the substrate, and a crack-free nanocoating was built when the loading of nanocoating was increased to 6.3 mg cm^{-2}. The activity tests for oxidation of benzene showed that 40 ppm gaseous benzene was converted to CO_2 with high selectivity (85%) at the low cell voltage of 2.0 V in this all-solid cell. The conversion of benzene was greatly increased from 30% to 100% upon increasing the Sb/Sn ratio of the nanocoating from 4.7 mol% to 14.0 mol%. With the increase of nanocoating loading (Sb/Sn = 14.0 mol%) from 6.3 to 7.7 mg cm^{-2}, the conversion of 100 ppm benzene was increased from 70% to 100%. Cyclic voltammetry revealed that high Sb content in the oxide nanocoating increased the overpotential and current intensity of the oxygen evolution reaction. The large outer charge q_o^* related to the electroactive surface of the SS-7.7/Ti3 electrode was up to 305.3 mC cm^{-2}, which were responsible for its excellent electrochemical performance in the benzene oxidation process. Our studies provide a potential method for removal of indoor VOCs at ambient temperature.

1. Introduction

Benzene, toluene and xylene (BTX) are important raw materials emitted from a variety of industrial and commercial processes (Weschler, 2009; World Health Organization, 2000). As major components of volatile organic compounds (VOCs), BTX promote the formation of haze in the atmosphere and have high toxic potential toward human beings (Jones, 1999). Various kinds of techniques are available for removing BTX from polluted air, including adsorption, thermal combustion, catalytic combustion, photocatalysis and plasma oxidation (Meng et al., 2013; Dai, 2015; Luengas et al., 2015; Zhang et al., 2016; Stoll et al., 2017). However, secondary pollution and operational risk are inevitable in these removal processes. Therefore, BTX mineralization at ambient temperature in indoor and outdoor air is still a challenge.

Electrochemical oxidation has been successfully applied for mineralization of aromatic organics in water treatment, since it

* Corresponding author. State Key Joint Laboratory of Environment Simulation and Pollution Control, Research Center for Eco-Environmental Sciences, Chinese Academy of Sciences, Beijing 100085, China.
E-mail address: cbzhang@rcees.ac.cn (C. Zhang).

https://doi.org/10.1016/j.chemosphere.2018.10.222
0045-6535/

provides a versatile, efficient and "clean reagent" process (Comninellis, 1994; Rajeshwar, 1994; Panizza and Cerisola, 2009; Antonin et al., 2015). In electrooxidation, pollutants are oxidized at anode surfaces through both direct and indirect mechanisms. Direct oxidation of pollutants at the anode requires suitable electrode materials to obtain vigorous oxidation conditions, which usually exhibit high overpotentials. Indirect electrooxidation occurs via hydroxyl radicals generated from water discharge on the surface of the anode (Comninellis, 1994; Antonin et al., 2015). Dimensionally stable anodes (DSA) (Kotz et al., 1991; Chen et al., 2001; Montilla et al., 2004; Liu and Feng, 2009; Zhao et al., 2009; Ciriaco et al., 2011; Hu et al., 2011; Costa and Da Silva, 2012; Berenguer et al., 2014; Da Silva et al., 2014; Goncalves et al., 2014; Shao et al., 2014; Yang et al., 2014, 2015) have received much attention due to their advantages of high catalytic activity for oxidation of organic pollutions, simple preparation methods and low cost. Among these, antimony-doped SnO_2 (Sb-SnO_2) is regarded as the most effective anode material for the electrochemical oxidation of organic pollutants in wastewater due to its excellent electrocatalytic performance (Kotz et al., 1991; Chen et al., 2001; Montilla et al., 2004; Liu and Feng, 2009; Zhao et al., 2009; Ciriaco et al., 2011; Hu et al., 2011; Berenguer et al., 2014; Da Silva et al., 2014; Goncalves et al., 2014; Shao et al., 2014; Yang et al., 2014, 2015). On the surface of SnO_2, the first step in the discharge of water is the formation of adsorbed •OH. Recently, Da Silva et al. (2014; Goncalves et al., 2014) obtained •OH from pure water electrolysis on Sb-SnO_2 anodes without the presence of an aqueous electrolyte, which demonstrated that the water discharge process to produce •OH can proceed without an aqueous conducting medium. Also, we directly measured •OH generated from water vapor discharge in an all-solid cell by laser-induced fluorescence techniques (Zhang et al., 2018). These results demonstrated that a conducting medium is not needed to achieve water or water vapor discharge to produce •OH. Moreover, collisions of •OH with ions are also avoided by the lack of a conducting medium. Doping with Sb enhances the conductivity of SnO_2 and increases the oxygen evolution overpotential (about 1.9 V vs SHE). The relatively high oxygen evolution potential hinders the combination of adjacent adsorbed •OH to form O_2. Therefore, an accumulation of •OH on the SnO_2 surface occurs, which contributes to the oxidation of organic compounds by the highly reactive •OH radicals (Panizza and Cerisola, 2009). Several studies (Kotz et al., 1991; Panizza and Cerisola, 2009; Da Silva et al., 2014; Goncalves et al., 2014) have investigated the effect of Sb content on the oxygen vacancies, conductivity, the overpotential of OER and the service life of the electrode. However, the conclusions of these studies were diverse. Da Silva et al. (Costa and Da Silva, 2012; Da Silva et al., 2014; Goncalves et al., 2014) investigated antimony-doped SnO_2 supported on fine-mesh substrates with Sb content in the range of 0–25.50 mol%, and concluded that the service life of the electrode depended on the Sb content, and that an electrode containing 15.46 mol% Sb had the maximum service life in electrolysis of water in a solid polymer electrolyte filter-press cell. However, they found that an electrode with 6.57 mol% Sb had the highest combustion rate for organic dye and was more stable than other electrodes due to the high mass-transport coefficient of the microstructure of the oxide surface. Kotz et al. (1991) found that the doping level of Sb had no significant influence on the overpotential of OER, and that an electrode with 5 mol% Sb had the lowest resistivity. Clearly, the influence of Sb content in SnO_2 on the electrochemical performance of electrodes depended on the electrochemical system studied. Although extensive studies have been performed on Ti/Sb-SnO_2 electrodes for the electrochemical oxidation of organic pollutants in wastewater, to our knowledge, studies regarding the electrooxidation of gaseous aromatics on Ti/Sb-SnO_2 electrodes are scarce. The effects of various parameters including Sb content, the loading weight of the oxide coating and the textural properties of the Ti substrate on the electrochemical behavior for oxidation of BTX have yet to be investigated.

In the present work, a facile and effective electrochemical oxidation process for BTX in an all-solid cell has been designed. Antimony-doped tin dioxide deposited on porous titanium foam (Sb-SnO_2/Ti) was used as the dimensionally stable anode, and reduced graphene oxide/carbon fiber paper-supported Pt (Pt/rGO/CFP) was employed as the cathode. The anode and cathode were compressed closely against a solid polymer electrolyte to form the membrane electrode assembly.

2. Experiments

2.1. Preparation of the Sb-SnO_2/Ti anode

We selected three foam Ti substrates with the pore sizes of 37.6 μm, 54.6 μm and 62.1 μm, and these substrates are denoted as Ti1, Ti2 and Ti3, respectively. All substrates had a thickness of 2.0 mm. These substrates were first polished with abrasive paper and etched with a 10% oxalic acid solution for 2 h. Then the substrates were washed with doubly distilled water by ultrasonic washing. Sb-SnO_2 was loaded onto the titanium foam plate by two steps, including an electrodeposition-calcination process and a brush coating-pyrolysis process. Electrodeposition of a mixture of Sn and Sb on the Ti foam plate was carried out at room temperature using a two-electrode system (1 cm separation) with the Ti foam plate serving as the cathode and Pt sheet serving as anode. An ethanediol solution containing 1 M $SnCl_4$, 0.2 M $SbCl_3$ and 0.1 M HNO_3 was used as the electroplating bath with a current density of 15 mA cm^{-2} for 1 h. After electrodeposition of Sn and Sb, the electrode was heated in an oven at 773 K for 1 h then naturally cooled in air to avoid cracking of the oxide films, and the Sn/Sb oxide formed on the Ti foam substrate and the electrode was denoted as SS-ED/Ti. The loading weight of the Sb-SnO_2 coating was 7.7 mg cm^{-2}. A solution mixture of isopropanol and n-butanol containing 0.5 M $SnCl_4$, 0.02 M $SbCl_3$, 1 M HNO_3 and 0.01 M NaF was brushed on the SS-ED/Ti electrode. NaF, as a morphology controlling agent and conductive agent, can effectively improve the quality and electrical conductivity of deposited films, and reduces the corrosion rate of PbO_2 and SnO_2 films in aqueous solution (Kong et al., 2012; Qiao et al., 2015; Wang et al., 2014). Additionally, NaF doping in PbO_2 and SnO_2 electrodes shifts the oxygen evolution reaction toward positive potential, which enables the generation of much more •OH and improves the current efficiency for the combustion/conversion reaction. Therefore, NaF was employed as an additive in the SnO_2 precursor solution in this study. After brush-coating, the sample was dried in an oven at 373 K for 10 min and then calcined at 773 K for 30 min, and then naturally cooled in air. The brush coating procedures were repeated until the loading amount of the brush-coating on the electrodes attained 4.4, 6.3 and 7.7 mg/cm^2, and the samples were referred to as SS-4.4/Ti, SS-6.3/Ti and SS-7.7/Ti, respectively. The geometric area of the prepared electrodes was 14.0 cm^2 (including both sides).

2.2. Preparation of the Pt/rGO/CFP cathode

The CFP substrate was made of 8–10 μm carbon fiber, which was first immersed in a 0.1 wt% Triton X-100 solution for 24 h and then ultrasonically treated in deionized water to reduce the hydrophobicity. Then, it was heated at 400 °C for 5 h to increase the number of oxygen-containing functional groups on the surface and thereby increase the impregnation in the 2 mg/mL GO dispersion. Subsequently, the GO film-coated CFP was immersed in a 10 mg/mL ascorbic acid solution overnight at room temperature. After

repeated rinsing with deionized water, a uniform rGO-coated CFP was obtained, which was used for electrodepositing Pt nanoparticles from an aqueous solution of 10 mM NH_4Cl containing 1 mM $PtCl_4$ (pH = 1) at a constant current of 20 mA for 120 min. The concentration of Pt^{4+} in the electrolyte was measured by an 8300 inductively coupled plasma optical emission spectrometer (ICP-OES, PerkinElmer Inc.) to quantify the Pt loading amount on the cathodes. The loading amount of Pt on the Pt/rGO/CFP electrode was determined to be 0.9 mg/cm^2.

2.3. Physicochemical characterization of electrodes

The morphology of the antimony-doped SnO_2 composite was observed by scanning electron microscopy (SEM, Merlin, Carl Zeiss, Germany) coupled with energy dispersive spectroscopy (X-MAX, Oxford Instruments). The crystalline structures of the composites were investigated by an X'Pert PRO powder diffractometer (XRD, Rigaku D/max, Rigaku Co.) using Cu Kα radiation scanning from 10° to 90° (2θ). X-ray photoelectron spectroscopy (XPS) was conducted on a scanning X-ray microprobe (Axis Ultra, Kratos Analytical Ltd.) with Al Kα radiation (1486.7 eV) to determine the surface composition and chemical state of the composite. The C1s peak (284.8 eV) was used to calibrate the binding energy (BE) values. The textural structure of electrodes was analyzed using an AutoPore IV 9510 mercury porosimeter (Micromeritics Instrument Co.). The concentrations of Sn^{4+} and Sb^{3+} in the electrolyte were measured by an 8300 inductively coupled plasma optical emission spectrometer (ICP-OES, PerkinElmer Inc.) to quantify the Sn and Sb loading amounts on the anodes.

2.4. Electrochemical oxidation tests for benzene

2.4.1. Setup

The schematic diagram of the experimental setup is shown in Fig. 1. The testing system consisted of an all-solid reactor, an anodic reactant gas reservoir with 2.0 L volume, cathodic gas flow of 20% O_2 in N_2, a CHI 760E electrochemical workstation (CH Instrument. Co. Ltd., Shanghai China), and a gas chromatograph. The all-solid reactor was separated into two compartments by the membrane electrode assembly (Fig. SM-1 in supplementary information (SM)). A pressure of 0.6 MPa cm^{-2} was applied to compress the anode and cathode against the solid polymer electrolyte to prevent gaps and membrane cracking. Each compartment of the all-solid reactor was fed with gaseous streams at a flow rate of 100 mL min^{-1}. The anodic reactant mixture containing H_2O vapor and concentrated benzene was recirculated via a pump from the gas reservoir, flowing through the reactor and the detector. The benzene was supplied by cylinder gas (Beijing Huayuan Gas Chemical Co., Ltd.). The reactant gases in the anodic compartment contained 40 ppm benzene, O_2 (20%) and N_2 balance with relative humidity varying from 0 to 60%. The relative humidity was regulated by adjusting the flow of dry feed gas bubbled through a humidity control unit including a cold-water circulation apparatus (CCA-20, Gongyi Yuhua Instrument Co., Ltd) and a hygrometer (314, Taiwan Center technology Co.), which controlled the temperature of the pure water in the bottle and monitored the humidity of the reactant stream.

The anodic reactants and products were analyzed online using a gas chromatograph (Shimadzu, GC 2014C) equipped with flame ionization detector (FID). A Rtx-Wax strongly polar capillary column was used for the high-sensitivity analysis of benzene series compounds, alcohols, aldehydes, acids and phenols. Two packed columns (Porapak-N and MS-13X) were equipped for the analysis of the anodic products CO_2 and CO. The reactants and the products were also monitored by a mass spectrometer (GAM200, InProcess Instruments).

Since benzene can be electro-oxidized to CO_2 and CO (CO_x), the overall process can be considered to occur as follows:

$$C_6H_6 + 6H_2O \rightarrow 6CO + 18H^+ + 18e^-$$

$$C_6H_6 + 12H_2O \rightarrow 6CO_2 + 30H^+ + 30e^-$$

$$\text{Benzene conversion } (\%) = \frac{C_0 - C}{C_0} \times 100$$

$$\text{CO or } CO_2 \text{ yield } (\%) = \frac{\Delta C_{cox}/6}{C_0} \times 100$$

where c_0 and c are the concentrations of benzene initially and at time t (ppm), respectively. Δc_{cox} is the experimental value for the CO or CO_2 yield at time t.

2.4.2. Electrochemical characterization

The cyclic voltammetry (CV) and linear sweep voltammetry (LSV) experiments were carried out on a CHI760e electrochemical workstation. All of the electrochemical measurements were performed using a three-electrode system in a two-compartment cell with Nafion 117 serving as the separator. The working electrodes were 2.0 cm diameter Sb-SnO_2/Ti. The counter electrode was a Pt rod of 1.0 cm length and 1.0 mm diameter. The reference electrode was a KCl-saturated Ag/AgCl electrode. The aqueous 0.5 M H_2SO_4 solutions were prepared with ultra-pure water with a resistivity of 18.2 MΩ cm^{-1} (Genpure Pro ultrapure water purification system, UV-TOC xCAD plus, Thermo scientific). For stability, the electrolyte was deoxygenated by N_2 bubbling with flow rate of 200 mL min^{-1}. In these studies, CV measurements were performed at a scan rate between 5 and 500 mV s^{-1}. The voltammetric charges (q*) corresponding to the electrochemically active surface areas were determined by integrating the area of the cyclic voltammograms.

3. Results

3.1. Characterization of the electrodes

To avoid the formation of a TiO_2 passivation layer, the freshly etched foam metal Ti was immediately immersed into the ethanediol electrolyte. Sn prepared by the electroreduction of Sn^{4+} covered the surface of the Ti substrate. After calcination in the air, SnO_2 was formed on the surface of the Ti foam substrate. As shown in Fig. 2a, the SS-ED/Ti electrode presents a compact microstructure with 57.5 nm SnO_2 nanoparticles, and the specific surface area of the electrode is increased compared with the Ti substrate, as shown in Table SM-1. In comparison, the size of SnO_2 particles on conventional Ti plate substrates in previous works was usually hundreds of nanometers (Montilla et al., 2004; Liu and Feng, 2009; Ciriaco et al., 2011; Berenguer et al., 2014). The current results are similar to the findings in a previous study (Hu et al., 2011), where the addition of the porous material Cr_3C_2 on the substrate was found to lead to the formation of SnO_2 nanoparticles. It is probable that the porous structure and the etched surface of the Ti substrate contributed to forming the nanoparticle coating.

The SS-ED/Ti electrodes were brush-coated with the Sn^{4+} and Sb^{3+} solution. After drying and calcination, three Ti/Sb-SnO_2 electrodes with Sb-SnO_2 loading weights of 4.4, 6.3 and 7.7 mg/cm^2 were obtained. As shown in Fig. 2b, numerous deep and wide cracks were present in the 4.4 mg/cm^2 Sb-SnO_2 coating. With increased loading, the coating cracks gradually disappeared, as seen in Fig. 2c and (d) and the coating on the 6.6 mg/cm^2 Ti/Sb-SnO_2 electrode shows a compact and crack-free appearance. Generally,

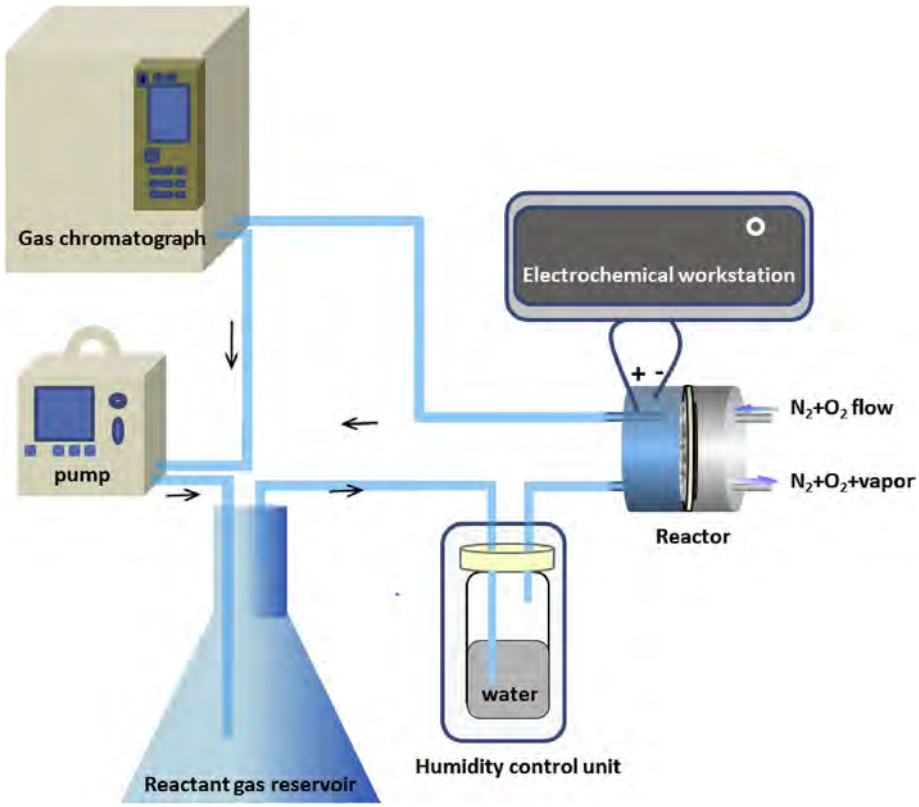

Fig. 1. Sketch of the experimental setup used in the electrochemical oxidation of benzene under flow conditions.

having a crack-free Sb-SnO_2 coating is important to the lifetime of electrode according to the deactivation mechanism, in which oxygen penetrate into the coating through the cracks, resulting in the formation of nonconductive TiO_2 (Shao et al., 2014). The interfacial stress between the coating and substrate caused the coating to peel off. In Fig. 2, the average size of nanoparticles rose with the increase of loading weight. It is likely that SnO_2 crystal seeds initially formed on the SS-ED/Ti electrode, which then grew with the repeated brush coating-pyrolysis process. In Fig. 2(d4)-(d8), the mapping images of the SS-7.7/Ti electrode show that Sn and Sb are homogeneously distributed in the oxide nanocoating on the Ti foam surface. The content of Sb in the coating is about 5 mol%.

Fig. SM-2 shows the X-ray diffraction patterns of Sb-SnO_2 supported on two types of Ti substrates. The Ti plate was completely covered by the coating, and strong diffraction peaks of cassiterite SnO_2 (PDF# 41–1445) were detected on SS-7.7/Ti-plate (Chen et al., 2001; Liu and Feng, 2009; Berenguer et al., 2014; Shao et al., 2014). No additional peaks appeared corresponding to antimony oxides, perhaps due to the low doping level or the incorporation of Sb in the SnO_2 unit cell. In contrast, no characteristic diffraction peaks of Sn and Sb oxides appear in the XRD of coatings formed on the Ti foam substrate, even with the high loading of 7.7 mg/cm^2 Sb-SnO_2. As shown in Fig. 2 (d8), the signal of the Ti substrate was detected, exhibiting that the thickness of the coating was lower than 500 nm (detection limits of EDS).

The surface composition and chemical state of the elements were analyzed by X-ray photoelectron spectroscopy. Fig. 3a shows the Sn (3d) spectra of electrodes with different loading weights of coating. Two peaks were observed at 487 and 495 eV, typically assigned to the Sn $3d_{5/2}$ and $3d_{3/2}$ states, respectively, which are consistent with SnO, SnO_2 or $Sn(OH)_x$ species (Montilla et al., 2004; Yang et al., 2015). The binding energies of Sn in SS-6.3/Ti and SS-7.7/Ti are 487.5 and 495.9 slightly higher than that of SS-ED/Ti and SS-4.4/Ti (487.0 and 495.4), possibly suggesting that the oxidation state of Sn was increased in SS-6.3/Ti and SS-7.7/Ti. In Fig. 3b, the binding energy of Sb $3d_{3/2}$ at 540.4 eV indicated the presence of Sb_2O_5 (Montilla et al., 2004) in the nanocoating on the electrodes.

The elemental compositions estimated from XPS are shown in Table 1. It can be seen that the molar ratio of Sb/Sn in SS-ED is 4.8%. After the brush-coating process, the molar ratio of Sb/Sn increased from 5.7% for SS-4.4/Ti to 14.0% for SS-6.3/Ti and SS-7.7/Ti. The Sn content of the electrode is considerably less than that in the precursor solutions (the molar ratio of Sn/Sb = 25:1), which is attributed to sublimation of the $SnCl_4$ precursor at the high calcination temperature of 500 °C (Comninellis and Vercesi, 1991). In addition, the Sb content measured by XPS is much higher than that by EDS. The explanation for this result is that the Sb content in the surface of the coating is different from that in the bulk. EDS measures the bulk elemental composition of the nanocoating, while the maximum detection depth of XPS is only 5–10 nm (Chen et al., 2001). Accordingly, the XPS analysis results represent the elemental concentrations at the nanocoating surface. From the Sb content in the surface and bulk of the nanocoating, it can be concluded that the Sb was preferentially enriched on the surface of the coating.

From Fig. 3a and Table 1, the binding energy of Sn in SS-ED/Ti, SS-4.4/Ti and SS-6.3/Ti increases with the increase of Sb content in the nanocoating. Additionally, the binding energy of Sn in SS-6.3/Ti is the same as that of SS-7.7/Ti with the same Sb concentration of 14.0 mol%. These results indicate that the Sb doping probably influences the oxidation state of Sn. An increase in the Sb content can promote the formation of high valence tin oxide SnO_2 on the surface of the electrode. It is generally known that Sn (IV) is the highest oxidation state of tin in oxides. The •OH radicals generated from discharge of water cannot react with SnO_2 and instead physically adsorb and accumulate on the surface of SnO_2 (Panizza and

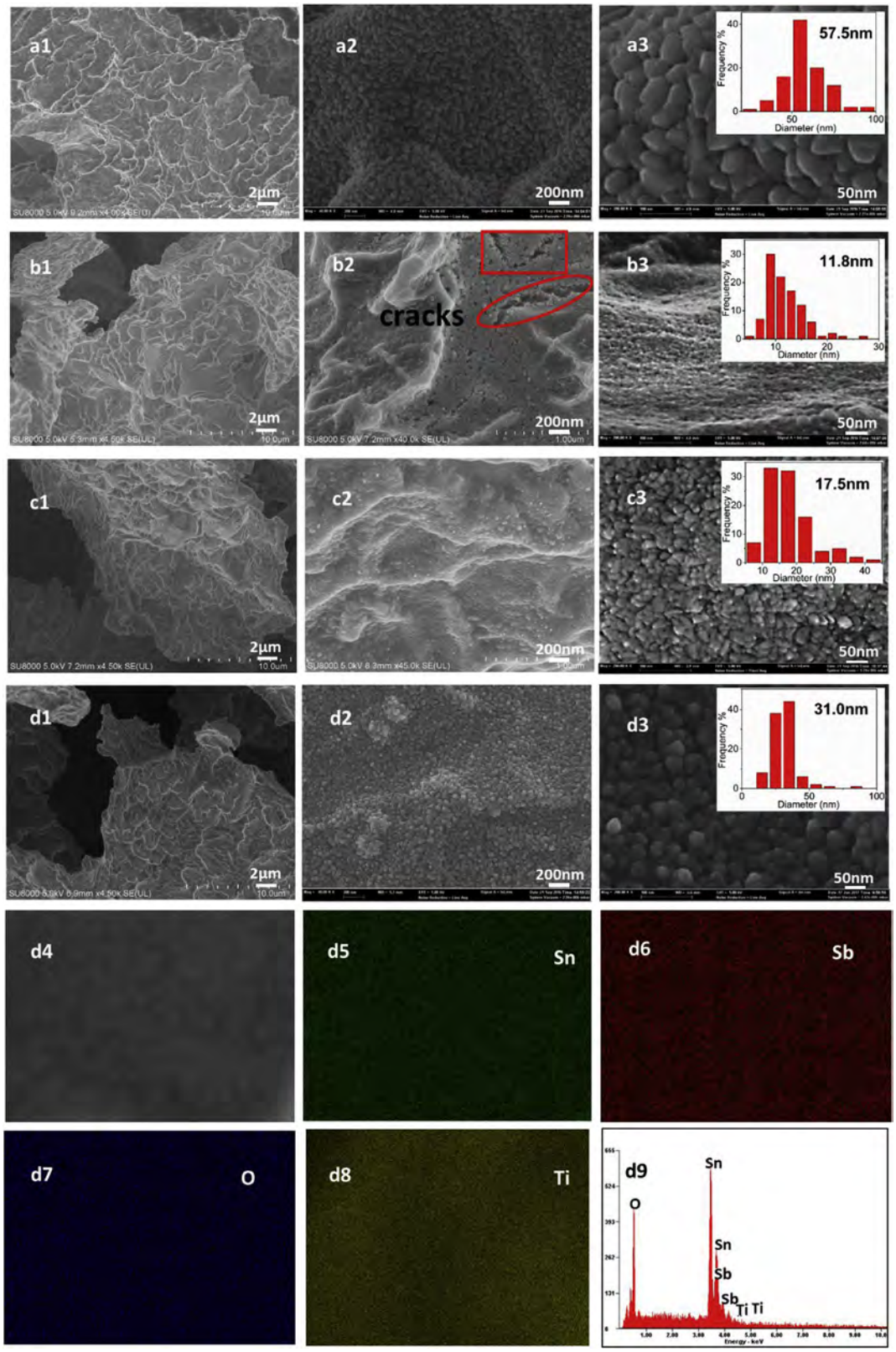

Fig. 2. SEM images of Sb-SnO_2/Ti anodes with loading weight of (a) SS-ED/Ti (b) SS-4.4/Ti1, (c) SS-6.3/Ti1 and (d1-d3) SS-7.7/Ti1. (d4-d8) secondary electron image and X-ray dot map of Sn, Sb and Ti, and (d9) elemental analysis scan.

Cerisola, 2009), which is beneficial for the oxidation of organics. Therefore, the increase of Sb in the SnO_2 nanocoating will improve the electrooxidation behavior of the electrode.

The textural properties of the electrodes were examined. As shown in Table SM-1, the pore diameter of the electrodes decreased with the loading weight of the coating, while the specific surface

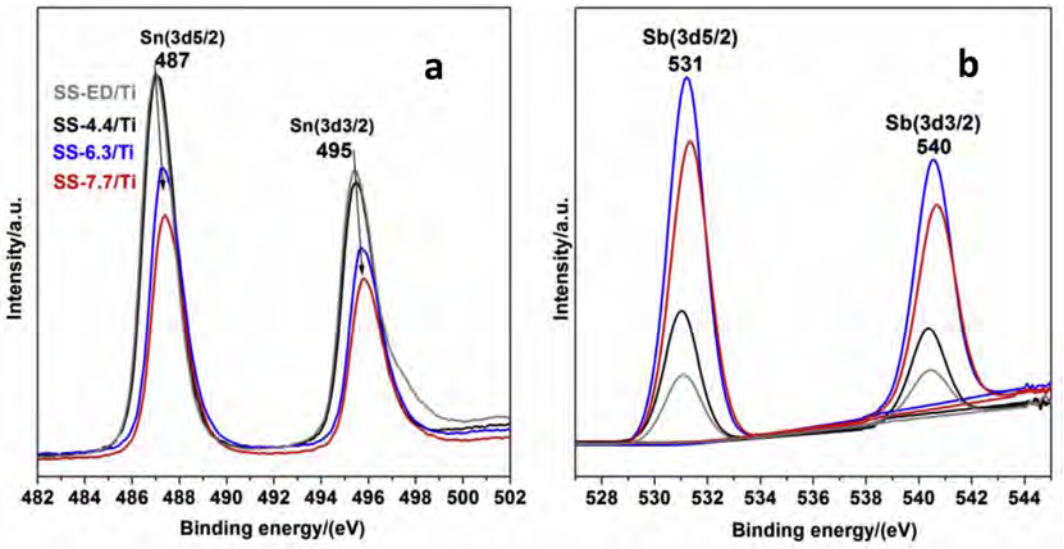

Fig. 3. XPS patterns of Sn and Sb 3d transition region of Sb-SnO_2/Ti anodes.

Table 1
Metal composition on the surface of antimony-doped SnO_2 coating on electrode.

Sample	Sn	Sb	O	C	Sb/Sn (mol%)
SS-ED/Ti	19.33	0.90	53.15	15.49	4.8
SS-4.4/Ti	15.11	0.91	58.03	8.30	5.7
SS-6.3/Ti	14.20	2.32	63.50	7.52	14.0
SS-7.7/Ti	10.27	1.68	63.27	6.64	14.0

areas of the electrodes were higher than that of the substrate. The surface areas of SS-4.4/Ti electrodes were higher than that of SS-ED/Ti, probably due to the small size of the nanoparticles. However, the average size of particles increased with the nanocoating loading. It can be seen that the surface area dropped off >95% from the loading of 4.4–7.7 mg cm^{-2}, indicating that increasing the loading weight of the coating significantly reduced the surface area and pore diameter of the electrode.

3.2. Electrochemical oxidation of benzene in all-solid cell

The electrocatalytic oxidation of benzene was performed. At 2.0 V cell voltage, the influence of the Sb-SnO_2 coating amount on the activity of the electrodes was first investigated. As shown in Fig. 4a, the removal percentage for 40 ppm benzene was only 35% for the SS-ED/Ti1 (Sb/Sn = 4.8%) after 7 h electrolysis. 100% benzene conversion was achieved on SS-6.3/Ti1 after 5 h electrolysis, and the high selectivity for CO_2 (85%) suggests that the increase of the loading weight of Sb-SnO_2 and the Sb content in the coating significantly improved the activity of the electrode. However, when the loading weight of Sb-SnO_2 increased to 7.7 mg cm^{-2}, the benzene removal and CO_2 yield decreased compared that of SS-6.3/Ti1. The probable reason is that the reduced pore diameter impeded the diffusion of gas, so that the activity of SS-7.7/Ti1 electrode decreased.

In the currently used indoor air purification technologies, such as photocatalysis and non-thermal plasma, byproduct formation is typically encountered. To analyze the gaseous products of benzene oxidation in this all-solid cell, mass spectrometry was performed. It was found that the byproducts of the oxidation of BTX were influenced by the electrodeposition time in the preparation process of electrodes, as shown in Fig. SM-3. In the preparation of anodes, Sb-SnO_2 was loaded onto the titanium foam plate by a two-step process, including an electrodeposition-calcination process and brush coating-pyrolysis process. As shown in Fig. SM-3, no gaseous organic byproducts were present after the electrochemical oxidation of benzene on the SS-7.7/Ti1 sample for which the electrodeposition time was 1 h. Therefore, the conditions "current density of 15 mA cm^{-2} for 1 h" mentioned in Section "2.1, Preparation of the Sb-SnO_2/Ti anode" are the optimized conditions. As shown in Fig. 4b, during the electrochemical oxidation of benzene, no organic byproducts were detected beyond the components of the feed gas with 2.0 V applied cell voltage and 60% humidity in the *m*/*z* range from 20 to 200. Hence, the electro-oxidation of gaseous organic pollutants by the gas-solid cell is suitable for indoor gaseous VOC elimination under ambient conditions. The all-solid cell can be installed in air purification equipment or air conditioning units in buildings, cars etc. However, as shown in Fig. 4b, about 15% of benzene was converted into CO. In future work, addition of different metal ions into the anode materials to promote the catalytic activity for CO oxidation will be investigated.

In Fig. 4a, benzene removal and CO_2 yield were not promoted when the loading weight of Sb-SnO_2 was 7.7 mg cm^{-2}. The probable reason is that the reduced pore diameter impeded the activity of the SS-7.7/Ti1 electrode. The activity of electrodes prepared on Ti foam substrates with different pore diameters for mineralization of benzene was investigated, as shown in Fig. 5a. For the nanocoating loading weight of 7.7 mg cm^{-2}, the benzene conversion and CO_2 yield increased with the pore diameter of the electrode and the surface area of the nanocoating. As anticipated, larger pore diameter improved the diffusion of gas. Larger surface area increased the contact between active sites and reactants and promoted the activity of electrodes. When the concentration of benzene was increased up to 100 ppm, SS-7.7/Ti3 showed higher activity for the conversion of benzene to CO_x compared with SS-6.3/Ti3. As shown in Fig. 5b, after 6-h electrolysis, the conversion of benzene on SS-7.7/Ti3 was 100%, while that of SS-6.3/Ti3 was 70%, exhibiting that increasing the loading of Sb-SnO_2 nanocoating with the same Sb content (Sb/Sn = 14.0 mol%) significantly improved the activity of the electrode. The current densities as a function of the electrolysis time have been added in Fig. SM-4. It can be seen that current density was increased with the loading of Sb-SnO_2 nanocoating. The electrical energy consumption for benzene mineralization on the SS-7.7/Ti3 electrode was 0.264 kWh g^{-1} at 50%

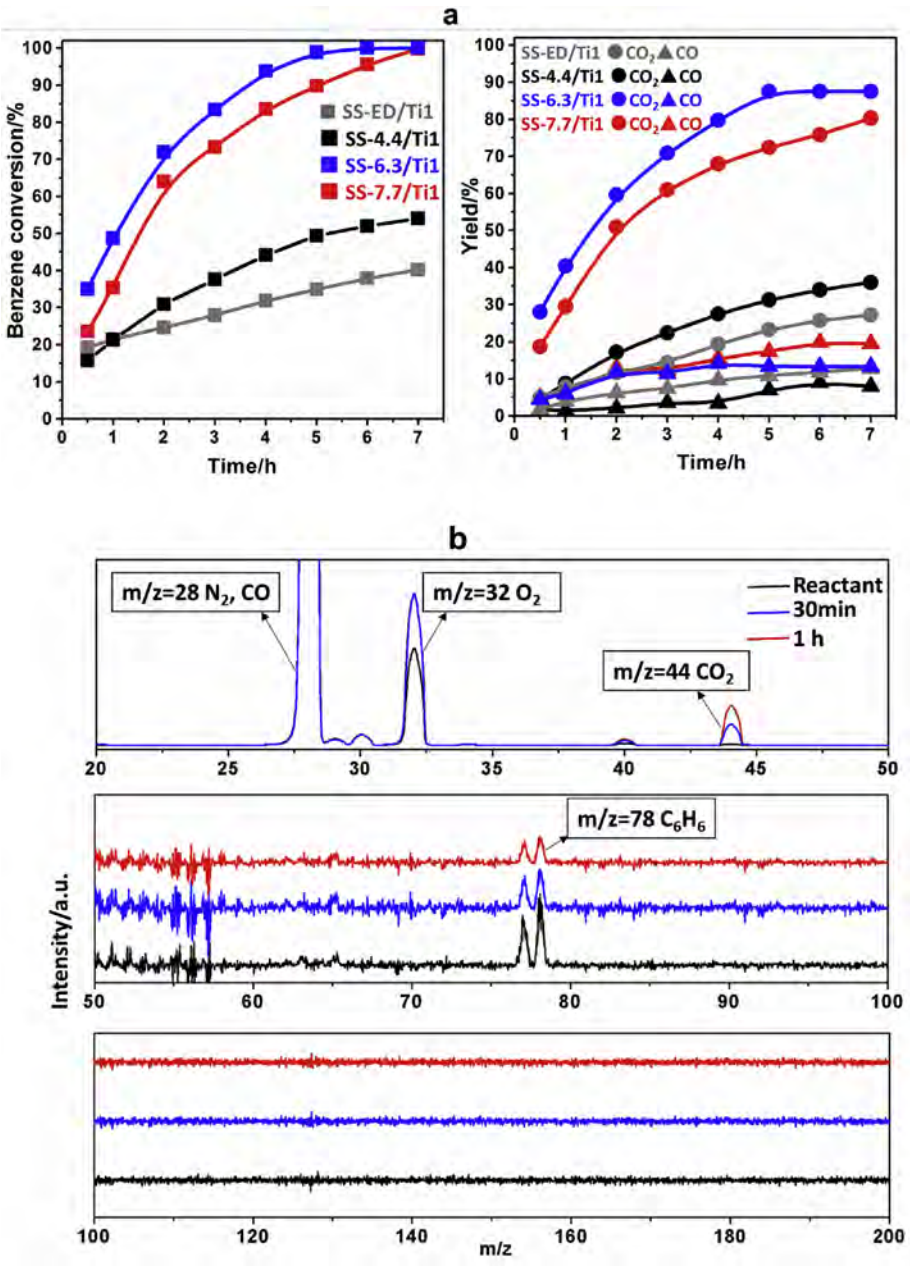

Fig. 4. Effects of the loading weight of Sb-SnO_2 on (a) the conversion of 40 ppm benzene to CO_x on Ti1-substrate electrodes with 2.0 V applied cell voltage at 60% RH. (b) Mass signals for reactant gas and gaseous products of benzene after electrolysis of 30 min and 1 h on SS-6.3/Ti1.

removal of 100 ppm benzene.

Without the electric field, the adsorption and conversion of benzene was analyzed for 7 h in RH 60% reactant gas. About 8% benzene were adsorbed on the anodic electrode in 7 h and no CO_x was generated, as shown in Fig. 5c. Benzene adsorption on the electrode increased in the absence of water vapor, indicating that competitive adsorption between water vapor and benzene occurred on the electrode. Additionally, when no water vapor was present in the reactant gas, 100% of the benzene was removed after 5 h, but no CO_x was produced, indicating that only adsorption or partial oxidation of benzene occurred on the anode and almost no direct oxidation of benzene occurred. It can be inferred that •OH generated from water vapor discharge played a major role in the oxidation of benzene at the cell voltage of 2.0 V. Compared with the high yield of CO_2 obtained (85%) at constant RH of 60%, the low yield of CO_2 (20%) shown when $RH_{ini} = 60\%$ (without additional water supply) also proved that the benzene oxidation was an indirect oxidation process. Moreover, continuous supply of water vapor to the reactant gas is important to the electro-oxidation of benzene. The anode service life of SS-7.7/Ti3 has been considered in our recently published paper (Zhang et al., 2018). The efficiency of benzene conversion remained almost constant from the first to the third run, and the CO_2 yield showed a moderate reduction from 80% to 70%. The reduction of selectivity for CO_2 may result from carbon accumulation on the surface of the electrode. In the future, we will carry out a study on improving the stability of the anode.

3.3. Electrochemical characterization

From the activity tests, it could be observed that benzene was oxidized mainly through the hydroxyl radicals generated from water vapor discharge on the surface of the anode. A high oxygen

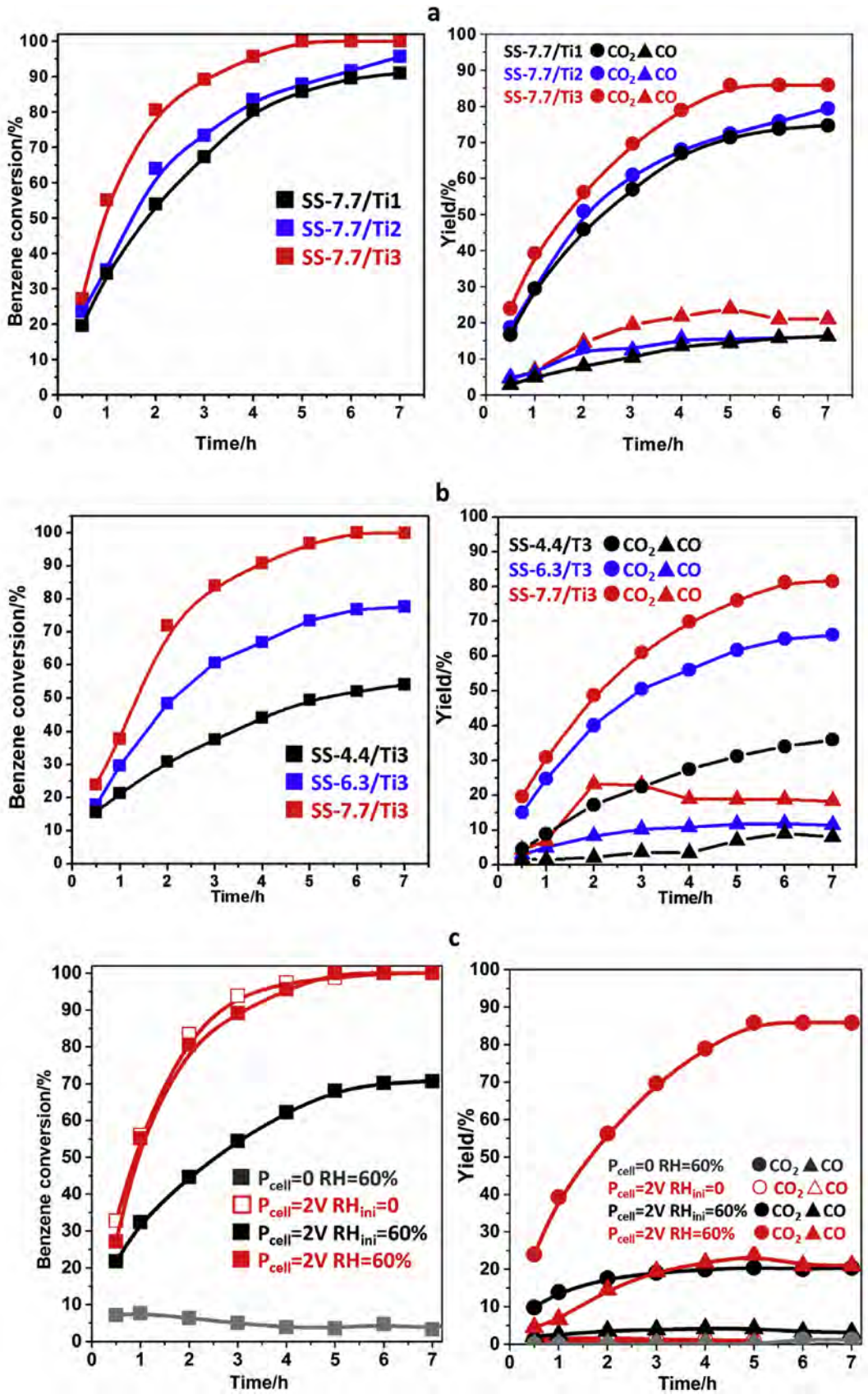

Fig. 5. (a) Effects of average pore size of substrate on the activity of electrodes for the conversion of 40 ppm benzene to CO_x with the RH of 60% at the cell voltage of 2.0 V. (b) The conversion of 100 ppm benzene to CO_x on SS-4.4/Ti3, SS-6.3/Ti3 and SS-7.7/Ti3 at the cell voltage of 2.0 V. (c) A comparison of benzene removal and CO_x yield on SS-7.7/Ti3 under various conditions. RH_{ini} is the initial relative humidity of the reactant gas. RH = 60% denotes that the relative humidity of the reactants was kept constant at 60% in the electrolysis.

evolution overpotential is helpful for accumulation of •OH on the electrode and beneficial to the "electrochemical incineration" of organic pollutants (Zhi et al., 2003; Li et al., 2005; Panizza and Cerisola, 2009; Hu et al., 2011). Therefore, the oxygen-evolution potential (OEP) is an important operational parameter for anode materials used in organic oxidation. The OEP of electrodes with different antimony doping levels in SnO_2 in 0.5 M H_2SO_4 were examined by voltammetric curves. The irreversible reduction of the tin oxide appeared at potentials less positive than 0.3 V, which caused electrode damage, and thus the potential limit must exceed 0.3 V. The subsequent extrapolation (dashed lines) of the current waves to 0 A was used to determine the OEP (vs Ag/AgCl). As shown in Fig. 6a, the onset potentials of anodic current were all higher than 1.45 V (vs Ag/AgCl). The OEP of SS-4.4/Ti3, SS-6.3/Ti3, and SS-7.7/Ti3 (1.84) was improved compared with that of SS-ED/Ti3 (1.78), and the current densities of these electrodes were greatly promoted with the increase of Sb content. The current densities of these electrodes at 1850 mV are shown in the inset of Fig. 6a. It can be seen that increasing Sb content in the electrodes (SS-ED/Ti3, SS-4.4/Ti3, SS-6.3/Ti3) greatly promotes the current density, suggesting that the addition of Sb improves the conductivity of the electrodes. When the Sb content was constant, the current density was similar in SS-6.3/Ti3 and SS-7.7/Ti3 electrodes. These results indicate that the Sb doping in SnO_2 nanoparticles improves the conductivity of electrodes and increases the overpotential of oxygen evolution.

Fig. 6b shows CV curves of electrodes for different antimony doping levels in SnO_2 at a scan rate of 50 mV s^{-1} in the potential window of 0.4–1.1 V. Obviously, the current density increased with the Sb content in the oxide coating. Additionally, at the Sb content of 14.0 mol%, the anodic and cathodic current density of SS-7.7/Ti3 were both greater than that of SS-6.3/Ti3. This indicates that the loading weight of the nanocoating on the electrode also influenced the current density of water discharge. The voltammetric charge ($q_T{}^*$) is related to the real surface area and the specific electroactivity of sites (Ardizzone et al., 1990; Baronetto et al., 1994; Berenguer et al., 2009, 2014). When the value of $q_T{}^*$ is larger, the electrochemical performance of an electrode is better. The voltammetric charge $q_T{}^*$ is obtained from the integral of the CV curves, and decreases with increasing potential scan rate ν. This is due to the fact that, at fast scan rate, the exchange of charged components between the solution and electroactive sites was hindered in the less-accessible sub-surface of the electrode. The relationship between $q_T{}^*$ and ν follows the equation (Ardizzone et al., 1990):

$$q_T{}^*(\nu) = q_o^* + k\nu^{-1/2}$$

Fig. 6c shows the relationship of $q_T{}^*$ versus the reciprocal square root of the scan rate $\nu^{-1/2}$ for electrodes. A good linear fit is observed. The $q_T{}^*$ at high scan rate (the value of outer charge, q_o^*) is the charge related to the most accessible electroactive surface, which can be obtained from the extrapolation to $\nu \to \infty$ in the plot of $q_T{}^*$ versus $\nu^{-1/2}$ (Montilla et al., 2004; Berenguer et al., 2009; Liu et al., 2017). For these electrodes, the outer charge q_o^* increased along with the Sb content and the loading weight of the oxide coating, as shown in Fig. 6c. SS-7.7/Ti3 has the highest q_o^*, indicating that it possesses the largest potential electroactive surface. The

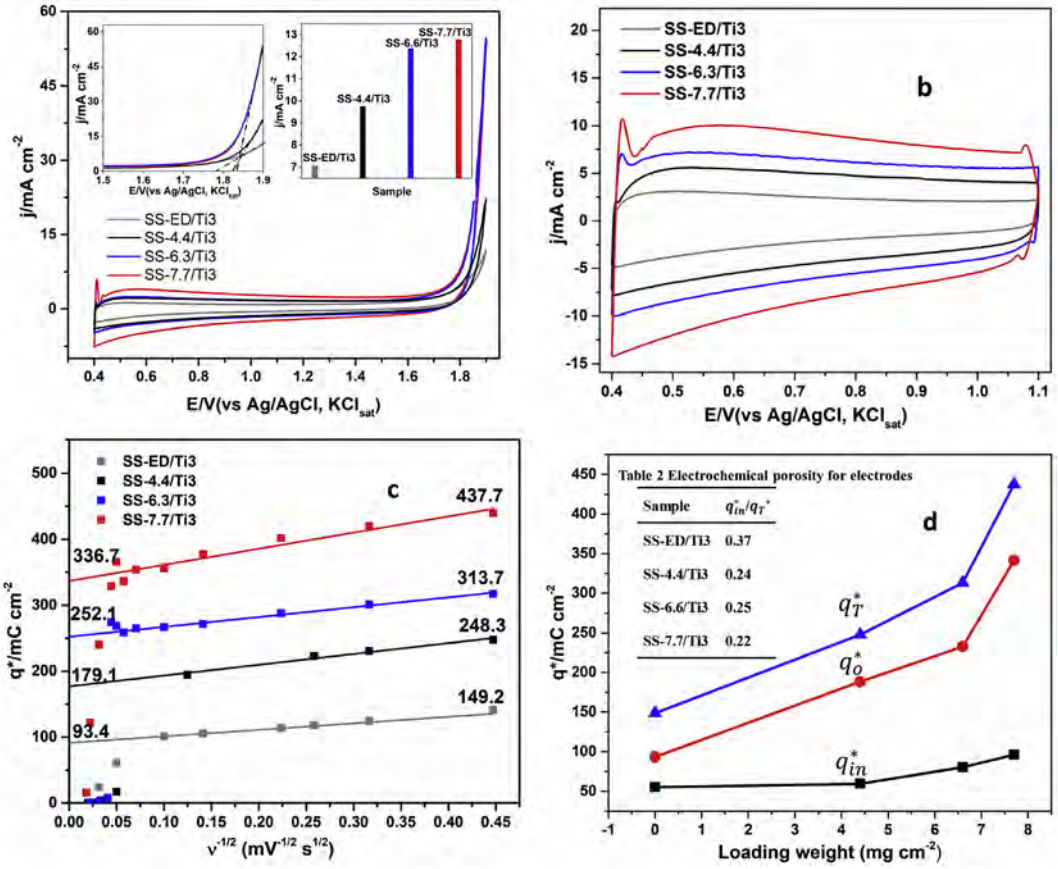

Fig. 6. (a) Cyclic voltammetric curves in 0.5 M H_2SO_4 at a scan rate of 20 mV s^{-1} on different electrodes after reaching steady state. (b) CV in 0.5 M H_2SO_4 at a scan rate of 50 mV s^{-1} on electrodes (c) the extrapolation of q_o^* for the electrodes from the plot of the voltammetric charge (q^*) versus the reciprocal square root of the voltammetric scan rate ($\nu^{-1/2}$). (d) Total ($q_T{}^*$), outer (q_o^*) and inner (q_{in}^*) charges for electrodes as a function of the loading weight of oxides. Electrochemical porosity for electrodes is shown in table 2 (insert in Fig. 6(d)). Data was obtained from the cycle voltammograms obtained between 0.4 and 1.1 V vs KCl saturated Ag/AgCl at various scan rates in 0.5 M H_2SO_4.

reaction constant k is the slope of the straight line in Fig. 6c, representing the increase in the reaction rate with decreasing scan rate. SS-7.7/Ti3 has a high k value of 297 mC $mV^{1/2}$ cm^{-2} $s^{-1/2}$. The inner voltammetric charge q_{in}^{*} corresponds to the less-accessible surface sites of the oxide layer, which can be calculated from the total charge and outer charge q_o^{*} ($q_T{}^{*}(\nu) = q_o^{*} + q_{in}^{*}$) (Baronetto et al., 1994). Fig. 6d shows the values of total charge, outer charge and inner charge as a function of the loading weight of the oxide layer. Obviously, the outer charge makes a large contribution to the total charge and increases with the loading weight of oxides and Sb content. The inner charge remains low and contributes little to the total charge. These results indicate that the loading weight and Sb content had the main influence on the electroactive surface of electrodes despite the differences of morphology observed by SEM. This is confirmed by the electrochemical porosity values obtained from the inner charge to total charge ratio ($q_{in}^{*}/q_T{}^{*}$) as shown in table 2 of Fig. 6d. It can be observed that the electrochemical porosities of these electrodes are of the same order of magnitude.

4. Conclusions

It was observed that benzene was oxidized to CO_2 with high selectivity in this all-solid cell at ambient temperature, indicating that this method is promising for indoor air purification applications. The electrochemical oxidation activity of the Sb-SnO_2/Ti foam nano-coating electrode for conversion of benzene to CO_x was significantly influenced by the Sb/Sn ratio and the loading weight of nanocoating. Continuous supply of water vapor was also important to benzene conversion. It was found that high Sb content in the oxide nanocoating increased the overpotential and the current intensity of the oxygen evolution reaction. The large electroactive surface of the SS-7.7/Ti3 electrode and the high reaction rate of water discharge on this electrode were responsible for its excellent electrochemical performance in the benzene oxidation process.

Acknowledgments

This work was financially supported by the National Key R&D Program of China (2017YFC0211802, 2016YFC0207104), and the National Natural Science Foundation of China (51678560, 21577159).

Appendix A. Supplementary data

Supplementary data to this article can be found online at https://doi.org/10.1016/j.chemosphere.2018.10.222.

References

Antonin, V.S., Santos, M.C., Garcia-Segura, S., Brillas, E., 2015. Electrochemical incineration of the antibiotic ciprofloxacin in sulfate medium and synthetic urine matrix. Water Res. 83, 31–41.
Ardizzone, S., Fregonara, G., Trasatti, S., 1990. Inner and outer active surface of RuO_2 electrodes. Electrochim. Acta 35, 263–267.
Baronetto, D., Krstajic, N., Trasatti, S., 1994. Reply to "Note on a method to interrelate inner and outer electrode areas" by H. Vogt. Electrochim. Acta 39, 2359–2362.
Berenguer, R., Quijada, C., Morallón, E., 2009. Electrochemical characterization of SnO_2 electrodes doped with Ru and Pt. Electrochim. Acta 54, 5230–5238.
Berenguer, R., Sieben, J.M., Quijada, C., Morallon, E., 2014. Pt- and Ru-doped SnO_2-Sb anodes with high stability in alkaline medium. ACS Appl. Mater. Interfaces 6, 22778–22789.
Chen, X.M., Chen, G.H., Yue, P.L., 2001. Stable Ti/IrOx–Sb_2O_5–SnO_2 anode for O_2 evolution with low Ir content. J. Phys. Chem. B 105, 4623–4628.
Ciriaco, L., Santos, D., Pacheco, M.J., 2011. Anodic oxidation of organic pollutants on a Ti/SnO_2-Sb_2O_4 anode. J. Appl. Electrochem. 41, 577–587.
Comninellis, C., Vercesi, G.P., 1991. Problems in DSA ® coating deposition by thermal decomposition. J. Appl. Electrochem. 21, 136–142.
Comninellis, C., 1994. Electrocatalysis in the electrochemical conversion/combustion of organic pollutants for waste water treatment. Electrochim. Acta 39, 1857–1862.
Costa, F.R., Da Silva, L.M., 2012. Fabrication and characterization of a porous gas evolving anode constituted of lead dioxide microfibers electroformed on a carbon cloth substrate. Electrochim. Acta 70, 365–374.
Da Silva, L.M., Goncalves, I.C., Teles, J.J.S., Franco, D.V., 2014. Application of oxide fine-mesh electrodes composed of Sb-SnO_2 for the electrochemical oxidation of Cibacron Marine FG using an SPE filter-press reactor. Electrochim. Acta 146, 714–732.
Dai, H.X., 2015. Environmental catalysis: a solution for the removal of atmospheric pollutants. Sci. Bull. 60, 1708–1710.
Goncalves, I.C., dos Santos, W.T.P., Franco, D.V., Da Silva, L.M., 2014. Fabrication and characterization of oxide fine-mesh electrodes composed of Sb-SnO_2 and study of oxygen evolution from the electrolysis of electrolyte-free water in a solid polymer electrolyte filter-press cell: possibilities for the combustion of organic pollutants. Electrochim. Acta 121, 1–14.
Hu, F., Dong, Z., Cui, X., Chen, W., 2011. Improved SnO_2–Sb_2O_4 based anode modified with Cr_3C_2 and CNT for phenol oxidation. Electrochim. Acta 56, 1576–1580.
Jones, A.P., 1999. Indoor air quality and health. Atmos. Environ. 33, 4535–4564.
Kong, H.S., Li, W., Lin, H., Shi, Z., Lu, H., Dan, Y., Huang, W., 2012. Influence of F^- doping on the microstructure, surface morphology and electrochemical properties of the lead dioxide electrode. Surf. Interface Anal. 45, 715–721.
Kotz, R., Stucki, S., Carcer, B., 1991. Electrochemical waste water treatment using high overvoltage anodes. Part I: physical and electrochemical properties of SnO_2 anodes. J. Appl. Electrochem. 21, 14–20.
Li, X., Cui, Y., Feng, Y., Xie, Z., Gu, J., 2005. Reaction pathways and mechanisms of the electrochemical degradation of phenol on different electrodes. Water Res. 39, 1972–1981.
Liu, J.F., Feng, Y.J., 2009. Investigation on the electrocatalytic characteristics of SnO_2 electrodes with nanocoating prepared by electrodeposition method. Sci. China Ser. E-Tech. Sci. 52, 1799–1803.
Liu, S., Wang, Y., Zhou, X., Han, W., Li, J., Sun, X., Shen, J., Wang, L., 2017. Improved degradation of the aqueous flutriafol using a nanostructure macroporous PbO_2 as reactive electrochemical membrane. Electrochim. Acta 253, 357–367.
Luengas, A., Barona, A., Hort, C., Gallastegui, G., Platel, V., Elias, A., 2015. A review of indoor air treatment technologies. Rev. Environ. Sci. Biotechnol. 14, 499–522.
Meng, Y.T., Genuino, H.C., Kuo, C.H., Huang, Chen, S.Y., Zhang, L.C., Rossi, A., Suib, S.L., 2013. One-step hydrothermal synthesis of manganese-containing MFI-type zeolite, Mn-ZSM-5, characterization, and catalytic oxidation of hydrocarbons. J. Am. Chem. Soc. 135, 8594–8605.
Montilla, F., Morallon, E., De Battisti, A., Barison, S., Daolio, S., Vazquez, J.L., 2004. Preparation and characterization of antimony-doped tin dioxide electrodes. 3. XPS and SIMS characterization. J. Phys. Chem. B 108, 15976–15981.
Panizza, M., Cerisola, G., 2009. Direct and mediated anodic oxidation of organic pollutants. Chem. Rev. 109, 6541–6569.
Qiao, Q., Wang, L., Shi, J., Jin, J., Li, Y., 2015. Properties of fluoride-doped β-PbO_2 electrodes and their electrocatalytic activities in degradation of acid orange II. Int. J. Electrochem. Sci. 10, 10639–10650.
Rajeshwar, K., 1994. Electrochemistry and the environment. J. Appl. Electrochem. 24, 1077–1091.
Shao, D., Li, X.L., Xu, H., Yan, W., 2014. An improved stable Ti/Sb–SnO_2 electrode with high performance in electrochemical oxidation processes. RSC Adv. 4, 21230–21237.
Stoll, T., Zafeiropoulos, G., Dogan, I., Genuit, H., Lavrijsen, R., Koopmans, B., Tsampas, M.N., 2017. Visible-light-promoted gas-phase water splitting using porous WO_3/$BiVO_4$ photoanodes. Electrochem. Commun. 82, 47–51.
Wang, J.T., Shi, X.L., Liu, W.W., Zhong, X.H., Wang, J.N., Pyrah, L., Sanderson, K.D., Ramsey, P.M., Hirata, M., Tsuri, K., 2014. Influence of preferred orientation on the electrical conductivity of fluorine-doped tin oxide films. Sci. Rep. 4 (3679), 1–9.
Weschler, C.J., 2009. Changes in indoor pollutants since the 1950s. Atmos. Environ. 43, 153–169.
World Health Organization (WHO), 2000. Air Quality Guidelines for Europe. World Health Organization, Geneva, Switzerland.
Yang, S.Y., Choi, W.Y., Park, H.W., 2015. TiO_2 nanotube array photoelectrocatalyst and Ni-Sb-SnO_2 electrocatalyst bifacial electrodes: a new type of bifunctional hybrid platform for water treatment. ACS Appl. Mater. Interfaces 7, 1907–1914.
Yang, S.Y., Kim, D., Park, H., 2014. Shift of the reactive species in the Sb-SnO_2-electrocatalyzed inactivation of *E. coli* and degradation of phenol: effects of nickel doping and electrolytes. Environ. Sci. Technol. 48, 2877–2884.
Zhang, B., Chen, M., Wang, L., Zhao, X., Hu, R., Chen, H., Xie, P., Zhang, C., He, H., 2018. Electrochemical oxidation of volatile organic compounds in all-solid cell at ambient temperature. Chem. Eng. J. 354, 93–104.
Zhang, Z., Jiang, Z., Shangguan, W., 2016. Low-temperature catalysis for VOCs removal in technology and application: a state-of-the-art review. Catal. Today 264, 270–278.
Zhao, G., Cui, X., Liu, M., Li, P., Zhang, Y., Cao, T., Li, H., Lei, Y., Liu, L., Li, D., 2009. Electrochemical degradation of refractory pollutant using a novel microstructured TiO_2 nanotubes/Sb-doped SnO_2 electrode. Environ. Sci. Technol. 43, 1480–1486.
Zhi, J.F., Wang, H.B., Nakashima, T., Rao, T.N., Fujishima, A., 2003. Electrochemical incineration of organic pollutants on boron-doped diamond electrode. Evidence for direct electrochemical oxidation pathway. J. Phys. Chem. B 107, 13389–13395.